

# Nodeless superconductivity in $\text{Ca}_3\text{Ir}_4\text{Sn}_{13}$ : evidence from quasiparticle heat transport

S. Y. Zhou, H. Zhang, X. C. Hong, B. Y. Pan, X. Qiu, W. N. Dong, X. L. Li, and S. Y. Li\*

*State Key Laboratory of Surface Physics, Department of Physics,  
and Laboratory of Advanced Materials, Fudan University, Shanghai 200433, P. R. China*

(Dated: October 17, 2018)

We report resistivity  $\rho$  and thermal conductivity  $\kappa$  measurements on  $\text{Ca}_3\text{Ir}_4\text{Sn}_{13}$  single crystals, in which superconductivity with  $T_c \approx 7$  K was claimed to coexist with ferromagnetic spin-fluctuations. Among three crystals, only one crystal shows a small hump in resistivity near 20 K, which was previously attributed to the ferromagnetic spin-fluctuations. Other two crystals show the  $\rho \sim T^2$  Fermi-liquid behavior at low temperature. For both single crystals with and without the resistivity anomaly, the residual linear term  $\kappa_0/T$  is negligible in zero magnetic field. In low fields,  $\kappa_0(H)/T$  shows a slow field dependence. These results demonstrate that the superconducting gap of  $\text{Ca}_3\text{Ir}_4\text{Sn}_{13}$  is nodeless, thus rule out nodal gap caused by ferromagnetic spin-fluctuations.

PACS numbers: 74.25.fc, 74.70.Dd

## I. INTRODUCTION

The interplay between magnetism and superconductivity has been a central issue in unconventional superconductors. While the static magnetism is generally believed to compete with superconductivity, the dynamic magnetism could be the source of electron pairing.<sup>1</sup> For example, the antiferromagnetic (AF) spin-fluctuations are considered as the pairing glue in high- $T_c$  cuprates, iron-based superconductors, and many heavy-fermion superconductors.<sup>1</sup> On another side, the ferromagnetic (FM) spin-fluctuations could be the origin of the superconductivity in  $\text{Sr}_2\text{RuO}_4$ , heavy-fermion superconductors  $\text{UGe}_2$  and  $\text{URhGe}$ .<sup>1</sup> These AF and FM spin-fluctuations usually result in superconducting gaps with nodes, such as the  $d$ -wave gap in cuprates and  $\text{CeCoIn}_5$ ,<sup>2,3</sup> and the  $p$ -wave gap in  $\text{Sr}_2\text{RuO}_4$ ,<sup>4</sup> but in some cases, such as the multiband iron-based superconductors, the AF spin-fluctuations may give  $s_{\pm}$ -wave gap without nodes.<sup>5</sup>

$\text{Ca}_3\text{Ir}_4\text{Sn}_{13}$  is a cubic transition metal compound, in which superconductivity with  $T_c \approx 7$  K was found thirty years ago.<sup>6</sup> Very few studies have been done on this compound since its discovery. Until recently, detailed resistivity, susceptibility, and specific heat measurements suggested that the superconductivity coexists with the FM spin-fluctuations in  $\text{Ca}_3\text{Ir}_4\text{Sn}_{13}$ .<sup>7</sup> A peak-like anomaly near 30 K in resistivity was observed. Below the anomaly, the non-Fermi-liquid behavior of resistivity in zero field has been attributed to the FM spin-fluctuations, and upon applying magnetic field, Fermi liquid behavior is recovered.<sup>7</sup>

Since the FM spin-fluctuations may cause a nodal superconducting state in  $\text{Ca}_3\text{Ir}_4\text{Sn}_{13}$ , it will be interesting to probe its superconducting gap structure. Ultra-low-temperature thermal conductivity measurement is such a bulk technique.<sup>8</sup> The existence of a finite residual linear term  $\kappa_0/T$  in zero magnetic field is an evidence for gap nodes. The field dependence of  $\kappa_0/T$  may further give support for a nodal superconducting state, and provide informations on the gap anisotropy, or multiple gaps.<sup>9</sup>

In this paper, we measure the resistivity and thermal conductivity of  $\text{Ca}_3\text{Ir}_4\text{Sn}_{13}$  single crystals. We find that while one crystal shows a small hump in resistivity near 20 K, other two crystals show  $\rho \sim T^2$  Fermi-liquid behavior in zero field. For both single crystals with and without the resistivity anomaly, the absence of  $\kappa_0/T$  in zero field and the slow field dependence of  $\kappa_0(H)/T$  in low fields clearly demonstrate nodeless superconductivity in  $\text{Ca}_3\text{Ir}_4\text{Sn}_{13}$ .

## II. EXPERIMENT

Single crystals of  $\text{Ca}_3\text{Ir}_4\text{Sn}_{13}$  were grown by flux method, as previously described in Ref. 6. The excessive Sn flux was etched in concentrated hydrochloric acid (HCl). The obtained single crystals have typical size of a few  $\text{mm}^3$ . We chose three single crystals with large flat surface, which was identified as (110) plane by X-ray diffraction measurements. Then the single crystals were polished and cut to a rectangular shape of typical dimensions  $2.5 \times 1.0 \text{ mm}^2$  in the (110) plane, and 0.2 mm in thickness. The dc magnetic susceptibility was measured in  $H = 20$  Oe both parallel and perpendicular to the (110) plane, using a SQUID (MPMS, Quantum Design). Four silver wires were attached on the sample with silver paint, which were used for both resistivity and thermal conductivity measurements, with electrical and heat currents in the (110) plane. The contacts are metallic with typical resistance 50 m $\Omega$  at 2 K. The thermal conductivity was measured in a dilution refrigerator, using a standard four-wire steady-state method with two  $\text{RuO}_2$  chip thermometers, calibrated *in situ* against a reference  $\text{RuO}_2$  thermometer. Magnetic fields were applied perpendicular to the (110) plane. To ensure a homogeneous field distribution in the sample, all fields were applied at temperature above  $T_c$ .

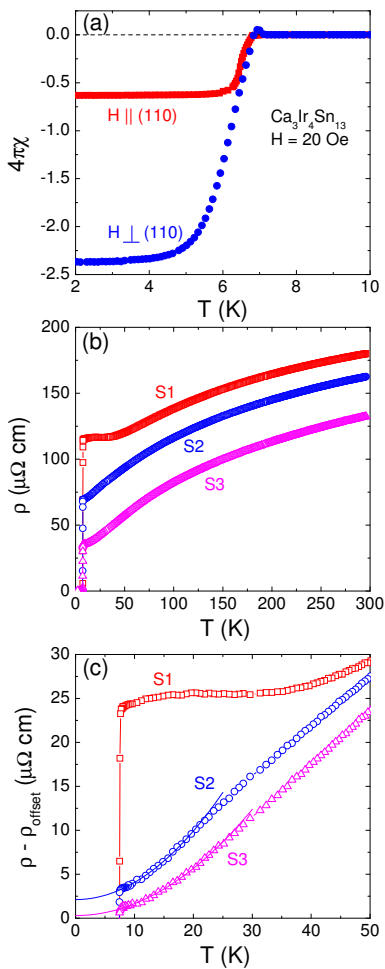


FIG. 1: (Color online) (a) The typical dc magnetic susceptibility of  $\text{Ca}_3\text{Ir}_4\text{Sn}_{13}$  single crystals measured in  $H = 20$  Oe both parallel and perpendicular to the (110) plane, with zero-field cooled. (b) Resistivity of three samples in zero magnetic field. (c) Low-temperature data of the resistivities in (b). The data sets are offset for clarity. Both samples S2 and S3 show  $\rho \sim T^2$  Fermi-liquid behavior at low temperature, as indicated by the solid lines.

### III. RESULTS AND DISCUSSION

Figure 1(a) presents the typical dc magnetic susceptibility of  $\text{Ca}_3\text{Ir}_4\text{Sn}_{13}$  single crystals, measured in  $H = 20$  Oe parallel and perpendicular to the (110) plane, with zero-field cooled. The transition temperature  $T_c \approx 6.9$  K is determined from the onset of diamagnetic transition. In field perpendicular to the (110) plane, the shielding volume fractions exceeds -1 at 2 K, indicating bulk superconductivity of the sample. Fig. 1(b) plots the resistivities of samples S1, S2, and S3 in zero magnetic field. For all three samples, the zero-resistivity  $T_c \approx 7.25$  K is slightly higher than that obtained from the magnetization measurements in Fig. 1(a), and the 10-90% resistive transition widths are less than 0.2 K.

From Fig. 1(b), only the resistivity of S1 shows an

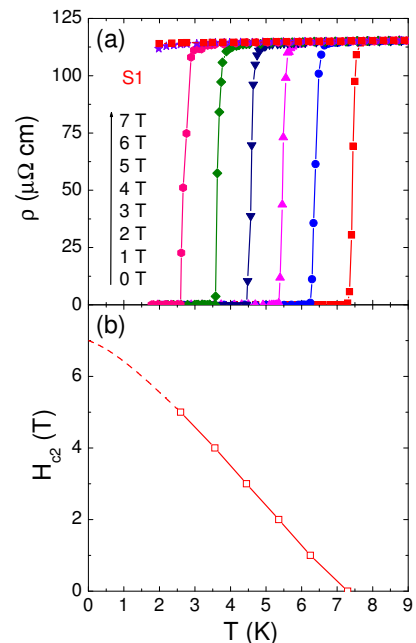


FIG. 2: (Color online) (a) Resistivity of  $\text{Ca}_3\text{Ir}_4\text{Sn}_{13}$  single crystal S1 in  $H = 0, 1, 2, 3, 4, 5, 6,$  and  $7$  T. The normal-state  $\rho(7\text{T})$  curve is quite flat, extrapolating to residual resistivity  $\rho_0(7\text{T}) \approx 114 \mu\Omega \text{ cm}$ . (b) Temperature dependence of the upper critical field  $H_{c2}$ , defined by  $\rho = 0$ . The dashed line is a guide to the eye, which points to  $H_{c2}(0) \approx 7$  T.

anomaly at low temperature, while S2 and S3 show good metallic behavior. Fig. 1(c) plots the resistivity data below 50 K. All data sets are offset for clarity. One can see that the small hump near 20 K of S1 is much less pronounced than the peak near 30 K in Ref. 7. Interestingly, for S2 and S3, the low-temperature data obey the Fermi-liquid behavior  $\rho \sim T^2$ , as indicated by the solid lines. We note that the residual resistivity  $\rho_0$  of S1 is the highest among all three samples. If lower  $\rho_0$  indicates higher sample quality, the resistivity anomaly may be not an intrinsic property of  $\text{Ca}_3\text{Ir}_4\text{Sn}_{13}$ . However, we are not sure about this at current stage.

Nevertheless, it is necessary to check the superconducting gap structure of both  $\text{Ca}_3\text{Ir}_4\text{Sn}_{13}$  samples with and without the resistivity anomaly. The upper critical field  $H_{c2}$  needs to be determined first. Fig. 2(a) shows the resistivity of  $\text{Ca}_3\text{Ir}_4\text{Sn}_{13}$  single crystal S1 in magnetic field up to  $H = 7$  T. For  $H = 7$  T, no superconducting transition is observed down to 2 K. The normal-state  $\rho(7\text{T})$  curve is quite flat, extrapolating to a residual resistivity  $\rho_0(7\text{T}) = 114.0 \mu\Omega \text{ cm}$ . In Fig. 2(b), we plot the temperature dependence of the upper critical field  $H_{c2}$ , defined by  $\rho = 0$  from the curves in Fig. 2(a). A rough estimation gives  $H_{c2}(0) \approx 7$  T. Similar measurements on S2 give the same  $H_{c2}(0)$ , and  $\rho_0(7\text{T}) = 79.6 \mu\Omega \text{ cm}$ .

Figure 3(a) shows the temperature dependence of the thermal conductivity for samples S1 and S2 in zero magnetic fields, plotted as  $\kappa/T$  vs  $T$ . The measured thermal conductivity is the sum of two contributions, respectively

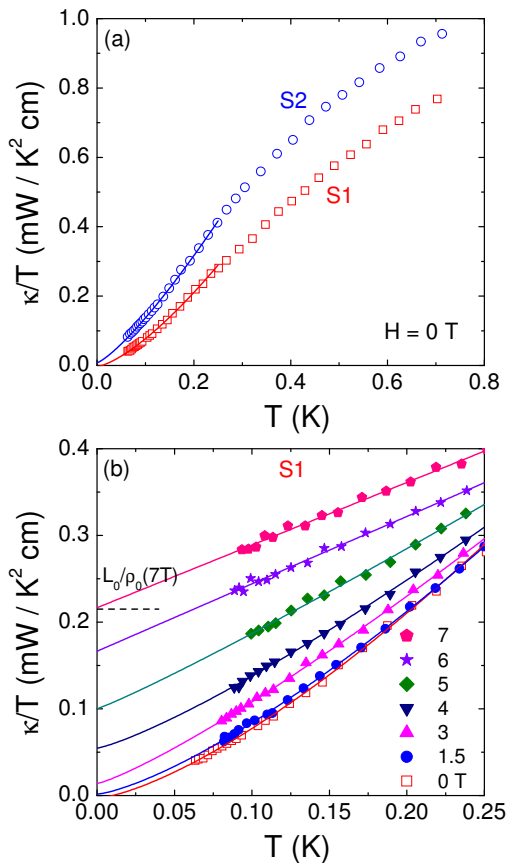


FIG. 3: (Color online) (a) Low-temperature thermal conductivity of  $\text{Ca}_3\text{Ir}_4\text{Sn}_{13}$  single crystals S1 and S2 in zero magnetic field. The solid lines are  $\kappa/T = a + bT^{\alpha-1}$  fits below 250 mK, respectively. (b) Thermal conductivity of S1 in magnetic fields. The dash line is the normal-state Wiedemann-Franz law expectation  $L_0/\rho_0(7\text{T})$ , with  $L_0$  the Lorenz number  $2.45 \times 10^{-8} \text{ W } \Omega \text{ K}^{-2}$  and  $\rho_0(7\text{T}) = 114.0 \mu\Omega \text{ cm}$ .

from electrons and phonons, so that  $\kappa = \kappa_e + \kappa_p$ . In order to obtain the residual linear term  $\kappa_0/T$  contributed by electrons, we extrapolate  $\kappa/T$  to  $T = 0$ . Usually, this can be done by fitting the data to  $\kappa/T = a + bT^{\alpha-1}$  at low temperature, where  $a \equiv \kappa_0/T$ .<sup>10,11</sup> The power  $\alpha$  of the second term contributed by phonons is typically between 2 and 3, due to specular reflections of phonons at the boundary.<sup>10,11</sup> From Fig. 3(a), the curves below 250 mK can be well fitted by  $\kappa/T = a + bT^{\alpha-1}$  with  $\alpha = 2.41$  and  $2.27$  for S1 and S2, respectively. Previously  $\alpha \approx 2.2$  has been observed in the *s*-wave superconductor  $\text{Cu}_{0.06}\text{TiSe}_2$ ,<sup>12</sup> and recently  $\alpha \approx 2$  was found in some iron-based superconductors such as  $\text{BaFe}_{1.9}\text{Ni}_{0.1}\text{As}_2$  and  $\text{KFe}_2\text{As}_2$ .<sup>13,14</sup> Below we will only focus on  $\kappa_0/T$ .

In zero field, the fittings give  $\kappa_0/T = -3 \pm 3$  and  $8 \pm 5 \mu\text{W K}^{-2} \text{ cm}^{-1}$  for S1 and S2, respectively. Note that our experimental error bar is about  $5 \mu\text{W K}^{-2} \text{ cm}^{-1}$ . For *s*-wave nodeless superconductors, there are no fermionic quasiparticles to conduct heat as  $T \rightarrow 0$ , since all electrons become Cooper pairs. Therefore there is no residual linear term of  $\kappa_0/T$ , as seen in  $\text{V}_3\text{Si}$ .<sup>10</sup> However, for

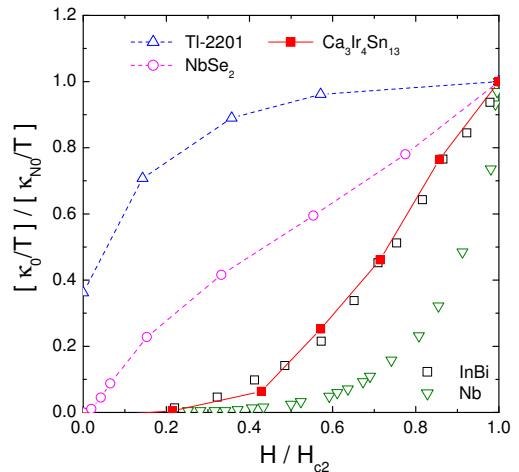


FIG. 4: (Color online) Normalized residual linear term  $\kappa_0(T)$  of  $\text{Ca}_3\text{Ir}_4\text{Sn}_{13}$  plotted as a function of  $H/H_{c2}$ . For comparison, similar data are shown for the clean *s*-wave superconductor Nb,<sup>16</sup> the dirty *s*-wave superconducting alloy InBi,<sup>17</sup> the multi-band *s*-wave superconductor NbSe<sub>2</sub>,<sup>18</sup> and an overdoped sample of the *d*-wave superconductor Tl-2201.<sup>19</sup>

unconventional superconductors with nodes in the superconducting gap, the nodal quasiparticles will contribute a finite  $\kappa_0/T$  in zero field.<sup>8</sup> For example,  $\kappa_0/T = 1.41 \text{ mW K}^{-2} \text{ cm}^{-1}$  for the overdoped cuprate  $\text{Tl}_2\text{Ba}_2\text{CuO}_{6+\delta}$  (Tl-2201), a *d*-wave superconductor with  $T_c = 15 \text{ K}$ .<sup>19</sup> For the *p*-wave superconductor  $\text{Sr}_2\text{RuO}_4$ ,  $\kappa_0/T = 17 \text{ mW K}^{-2} \text{ cm}^{-1}$ .<sup>15</sup> Therefore, the negligible  $\kappa_0/T$  of both S1 and S2 samples strongly suggests that the superconducting gap of  $\text{Ca}_3\text{Ir}_4\text{Sn}_{13}$  is nodeless.

Figure 3(b) plots the thermal conductivity of S1 in magnetic fields. All the curves are also fitted by  $\kappa/T = a + bT^{\alpha-1}$ . In  $H_{c2} = 7 \text{ T}$ ,  $\kappa_0/T = 0.216 \pm 0.003 \text{ mW K}^{-2} \text{ cm}^{-1}$  was obtained from the fitting. This value meets the Wiedemann-Franz law expectation  $L_0/\rho_0(7\text{T}) = 0.215 \text{ mW K}^{-2} \text{ cm}^{-1}$  nicely, with  $L_0$  the Lorenz number  $2.45 \times 10^{-8} \text{ W } \Omega \text{ K}^{-2}$  and  $\rho_0(7\text{T}) = 114.0 \mu\Omega \text{ cm}$ . The verification of Wiedemann-Franz law in the normal state shows the reliability of our thermal conductivity measurements.

As seen in Fig. 3(b),  $\kappa_0/T$  of S1 gradually increases with increasing field. In Fig. 4, we plot the normalized  $\kappa_0(H)/T$  as a function of  $H/H_{c2}$  for S1. The  $\kappa_0/T$  of S2 shows similar field dependence, which is not shown here. For comparison, the data of clean *s*-wave superconductor Nb,<sup>16</sup> the dirty *s*-wave superconducting alloy InBi,<sup>17</sup> the multi-band *s*-wave superconductor NbSe<sub>2</sub>,<sup>18</sup> and an overdoped sample of the *d*-wave superconductor Tl-2201<sup>19</sup> are also plotted. For a clean type-II *s*-wave superconductor with a single gap,  $\kappa$  should grow exponentially with field (above  $H_{c1}$ ), as is indeed observed in Nb.<sup>16</sup> For InBi, the curve is exponential at low  $H$ , crossing over to a roughly linear behavior closer to  $H_{c2}$  as expected for *s*-wave superconductors in the dirty limit.<sup>20</sup>

The normalized  $\kappa_0(H)/T$  of  $\text{Ca}_3\text{Ir}_4\text{Sn}_{13}$  clearly mimics that of the dirty *s*-wave superconductor InBi. However,

previously Yang *et al.* estimated the superconducting coherence length  $\xi_0 \sim 79$  Å and electronic mean free path  $l \sim 811$  Å, which implies that  $\text{Ca}_3\text{Ir}_4\text{Sn}_{13}$  is an intrinsic clean-limit superconductor ( $\xi_0 \ll l$ ).<sup>7</sup> Since the  $\rho_0$  of our sample S1 is about twice that of Yang *et al.*'s, we estimate the mean free path  $l \sim 400$  Å for S1. The  $H_{c2}(0)$  of S1 is the same as in Ref. 7, which gives the same  $\xi_0 \sim 79$  Å through the relation  $H_{c2}(0) = \Phi_0/2\pi\xi_0^2$ . Therefore sample S1 is still a clean superconductor, and the relatively fast increase of  $\kappa_0(H)/T$  near  $H_{c2}$  should have different origin from the dirty *s*-wave superconductor InBi.

Band structure calculation shows that there are six bands in  $\text{Ca}_3\text{Ir}_4\text{Sn}_{13}$  which cross the Fermi level.<sup>24</sup> Each sheet of the Fermi surface was found to be three dimensional, with rather complex shape.<sup>24</sup> In this context, we interpret the  $\kappa_0(H)/T$  behavior of  $\text{Ca}_3\text{Ir}_4\text{Sn}_{13}$  may result from multiple gaps or gap anisotropy.

For the multi-band *s*-wave superconductor  $\text{NbSe}_2$ ,  $\kappa_0(H)/T$  increases rapidly in both low field and near  $H_{c2}$ .<sup>18</sup> Similar behavior has been observed in  $\text{LNi}_2\text{B}_2\text{C}$  ( $L = \text{Y}, \text{Lu}$ ) with multiple and anisotropic gaps.<sup>21,22</sup> In both  $\text{NbSe}_2$  and  $\text{LNi}_2\text{B}_2\text{C}$ , applying a field rapidly delocalizes quasiparticle states confined within the vortices associated with the smaller gap band, while those states associated with the larger gap band delocalize more slowly. For  $\text{NbSe}_2$ , the ratio between larger and smaller gaps is approximately 3,<sup>23</sup> and for  $\text{YNi}_2\text{B}_2\text{C}$ , the ratio is about 2.1.<sup>22</sup> Recently, Bang has calculated the field dependence of  $\kappa_0(H)/T$  for different gap ratios, to explain the thermal conductivity data of multi-gap iron-based superconductor  $\text{Ba}(\text{Fe}_{1-x}\text{Co}_x)_2\text{As}_2$ .<sup>25</sup> It is possible that in  $\text{Ca}_3\text{Ir}_4\text{Sn}_{13}$ , the gaps in the six Fermi surfaces may have different magnitudes, or in some Fermi surface the gap is anisotropic. If this is the case, according to Bang's calculation,<sup>25</sup> the gap ratio in  $\text{Ca}_3\text{Ir}_4\text{Sn}_{13}$  should be around 1.4 or so. This interpretation needs to be

checked by momentum dependent measurements of the superconducting gap, such as angle-resolved photoemission spectroscopy (ARPES) experiments.

#### IV. SUMMARY

In summary, we report the resistivity and thermal conductivity measurements of  $\text{Ca}_3\text{Ir}_4\text{Sn}_{13}$  single crystals. Among three crystals, only one sample shows resistivity anomaly near 20 K, and other two samples display Fermi-liquid behavior  $\rho \sim T^2$  at low temperature. This suggests that the resistivity anomaly may be not intrinsic in  $\text{Ca}_3\text{Ir}_4\text{Sn}_{13}$ . Thermal conductivity results clearly demonstrate that the superconducting gap is nodeless in both crystals with and without the resistivity anomaly. This implies that the FM spin-fluctuations, if exist, may be irrelevant to the superconductivity in  $\text{Ca}_3\text{Ir}_4\text{Sn}_{13}$ , and the conventional electron-phonon interaction should be responsible for the electron pairing. The  $\kappa_0(H)/T$  shows a relatively fast increase near  $H_{c2}$ . Since  $\text{Ca}_3\text{Ir}_4\text{Sn}_{13}$  is not in the dirty limit, but rather has multiple Fermi surfaces with complex shape, we interpret that the behavior of  $\kappa_0(H)/T$  may result from gap anisotropy, or multiple isotropic gaps with different magnitudes.

#### ACKNOWLEDGEMENTS

This work is supported by the Natural Science Foundation of China, the Ministry of Science and Technology of China (National Basic Research Program No: 2009CB929203 and 2012CB821402), Program for Professor of Special Appointment (Eastern Scholar) at Shanghai Institutions of Higher Learning.

\* E-mail: shiyan\_li@fudan.edu.cn

- 
- <sup>1</sup> M. R. Norman, *Science* **332**, 196 (2011), and references therein.
- <sup>2</sup> C. C. Tsuei and J. R. Kirtley, *Rev. Mod. Phys.* **72**, 969 (2000).
- <sup>3</sup> K. An, T. Sakakibara, R. Settai, Y. Onuki, M. Hiragi, M. Ichioka, and K. Machida, *Phys. Rev. Lett.* **104**, 037002 (2010).
- <sup>4</sup> A. P. Mackenzie and Y. Maeno, *Rev. Mod. Phys.* **75**, 657 (2003).
- <sup>5</sup> P. J. Hirschfeld, M. M. Korshunov, and I. I. Mazin, *Rep. Prog. Phys.* **74**, 124508 (2011).
- <sup>6</sup> G. P. Espinosa, *Mater. Res. Bull.* **15**, 791 (1980). G. P. Espinosa, A. S. Copper, and H. Barz, *Mater. Res. Bull.* **17**, 963 (1982).
- <sup>7</sup> Jinhu Yang, Bin Chen, Chishiro Michioka, and Kazuyoshi Yoshimura, *J. Phys. Soc. Jpn.* **19**, 113705 (2010).
- <sup>8</sup> H. Shakeripour, C. Petrovic, and L. Taillefer, *New J. Phys.* **11**, 055065 (2009).
- <sup>9</sup> R. W. Hill, Shiyan Li, M. B. Maple, and Louis Taillefer, *Phys. Rev. Lett.* **101**, 237005 (2008).
- <sup>10</sup> M. Sutherland, D. G. Hawthorn, R. W. Hill, F. Ronning, S. Wakimoto, H. Zhang, C. Proust, E. Boaknin, C. Lupien, and Louis Taillefer, *Phys. Rev. B* **67**, 174520 (2003).
- <sup>11</sup> S. Y. Li, J.-B. Bonnemaïson, A. Payeur, P. Fournier, C. H. Wang, X. H. Chen, and L. Taillefer, *Phys. Rev. B* **77**, 134501 (2008).
- <sup>12</sup> S. Y. Li, G. Wu, X. H. Chen, and Louis Taillefer, *Phys. Rev. Lett.* **99**, 107001 (2007).
- <sup>13</sup> L. Ding, J. K. Dong, S. Y. Zhou, T. Y. Guan, X. Qiu, C. Zhang, L. J. Li, X. Lin, G. H. Cao, Z. A. Xu and S. Y. Li, *New J. Phys.* **11**, 093018 (2009).
- <sup>14</sup> J. K. Dong, S. Y. Zhou, T. Y. Guan, H. Zhang, Y. F. Dai, X. Qiu, X. F. Wang, Y. He, X. H. Chen, and S. Y. Li, *Phys. Rev. Lett.* **104**, 087005 (2010).
- <sup>15</sup> M. Suzuki, M. A. Tanatar, N. Kikugawa, Z. Q. Mao, Y. Maeno, and T. Ishiguro, *Phys. Rev. Lett.* **88**, 227004 (2002).
- <sup>16</sup> J. Lowell and J. B. Sousa, *J. Low. Temp. Phys.* **3**, 65 (1970).
- <sup>17</sup> J. O. Willis and D. M. Ginsberg, *Phys. Rev. B* **14**, 1916

- (1976).
- <sup>18</sup> E. Boaknin, M. A. Tanatar, J. Paglione, D. Hawthorn, F. Ronning, R. W. Hill, M. Sutherland, Louis Taillefer, J. Sonier, S. M. Hayden, and J. W. Brill, *Phys. Rev. Lett.* **90**, 117003 (2003).
- <sup>19</sup> C. Proust, E. Boaknin, R. W. Hill, Louis Taillefer, and A. P. Mackenzie, *Phys. Rev. Lett.* **89**, 147003 (2002).
- <sup>20</sup> C. Caroli and M. Cyrot, *Phys. Kondens. Mater.* **4**, 285 (1965).
- <sup>21</sup> E. Boaknin, R. W. Hill, C. Proust, C. Lupien, Louis Taillefer, and P. C. Canfield, *Phys. Rev. Lett.* **87**, 237001 (2001).
- <sup>22</sup> T. Baba, T. Yokoya, S. Tsuda, T. Watanabe, M. Nohara, H. Takagi, T. Oguchi, and S. Shin, *Phys. Rev. B* **81**, 180509(R) (2010).
- <sup>23</sup> T. Yokoya, T. Kiss, A. Chainani, S. Shin, M. Nohara, H. Takagi, *Science* **294**, 2518 (2001).
- <sup>24</sup> S. K. Goh, L. E. Klintberg, P. L. Alireza, D. A. Tompsett, Jinhu Yang, Bin Chen, K. Yoshimura, and F. Malte Grosche, arXiv:1105.3941 (2011).
- <sup>25</sup> Yunkyung Bang, *Phys. Rev. Lett.* **104**, 217001 (2010).